frontiers | Frontiers in Signal Processing

TYPE Original Research
PUBLISHED 28 January 2026
DOI 10.3389/frsip.2026.1712465

Check for updates

OPEN ACCESS

EDITED BY
Shalabh Gupta,
University of Connecticut, United States

REVIEWED BY
Amjad Humaidi,
University of Technology, Iraq, Iraq
Ankireddy Narendra,
Shri Mata Vaishno Devi University, India

*CORRESPONDENCE
Martin Valtierra-Rodriguez,
martin.valtierra@enap-rg.org

RECEIVED 24 September 2025
REVISED 28 December 2025
ACCEPTED 06 January 2026
PUBLISHED 28 January 2026

CITATION
Morales-Perez C, Amezquita-Sanchez JP, Rangel-Magdaleno J, Granados-Lieberman D and Valtierra-Rodriguez M (2026) Detection of inter-turn short circuits in induction motors using orthogonal matching pursuit and dictionary learning.
Front. Signal Process. 6:1712465.
doi: 10.3389/frsip.2026.1712465

COPYRIGHT
© 2026 Morales-Perez, Amezquita-Sanchez, Rangel-Magdaleno, Granados-Lieberman and Valtierra-Rodriguez. This is an open-access article distributed under the terms of the Creative Commons Attribution License (CC BY). The use, distribution or reproduction in other forums is permitted, provided the original author(s) and the copyright owner(s) are credited and that the original publication in this journal is cited, in accordance with accepted academic practice. No use, distribution or reproduction is permitted which does not comply with these terms.

Detection of inter-turn short circuits in induction motors using orthogonal matching pursuit and dictionary learning

Carlos Morales-Perez[1], Juan Pablo Amezquita-Sanchez[1], Jose Rangel-Magdaleno[2], David Granados-Lieberman[3] and Martin Valtierra-Rodriguez[1]*

[1]ENAP-Research Group, CA-Sistemas Dinámicos y Control, Facultad de Ingeniería, Universidad Autónoma de Querétaro (UAQ), Campus San Juan del Río, Querétaro, Mexico, [2]Digital Systems Group, Coordinación de Electrónica, Instituto Nacional de Astrofísica, Óptica y Electrónica (INAOE), Puebla, Mexico, [3]ENAP-Research Group, CA-Fuentes Alternas y Calidad de la Energía Eléctrica, División de Ingeniería en Electromecánica, Tecnológico Nacional de México, ITS Irapuato, Guanajuato, Mexico

Fault detection in induction motors is critical due to their extensive use in industrial applications. Among the various types of faults, stator faults are the most frequent and complex, making early detection particularly challenging. In this paper, a novel methodology for detecting inter-turn short circuits (ITSCs) through stator current analysis is presented. The methodology employs a sine–cosine filter to suppress the fundamental-frequency component, constructs a cumulative distribution function (CDF) to enhance ITSC-related features, and detects faults via a sparse representation of the CDF using the Orthogonal Matching Pursuit algorithm. To verify the methodology's effectiveness, the current stator signals have been analyzed across five levels of fault and four mechanical load conditions. Finally, experimental results show that the proposed method achieves a fault-detection accuracy of 98%, requires a small training dataset, and enables the detection of up to 10 short-circuited turns.

KEYWORDS

cumulative distribution function, fault detection, induction motor, inter-turns short-circuit, orthogonal matching pursuit, sparse representation, stator current signal, stator faults

1 Introduction

Rotary electrical machines have been the most essential machines in diverse areas of the industry. Among the different types of rotary machines, Induction Motors (IMs) have had a strong presence in the industry due to their low cost and reliability. These machines have substantial worldwide applications, accounting for an estimated 60%–80% of electrical energy consumption in the industrial sector (Gonzalez-Abreu et al., 2022; de Souza et al., 2022; Ghosh et al., 2020). As a crucial component of industrial processes, IMs must be continuously monitored to ensure its correct functionality, maximize its useful life, and prevent production process breakdowns.

Despite the promising results reported in the literature, faults in IMs and their detection are still a current and hot topic of research. In this regard, various authors have presented novel investigations in order to increase the viability and accuracy of fault detection and classification in line with the available technology and state-of-the-art methods. Additionally, research about the nature and locations of faults has enabled specific

methods thanks to the identification of intrinsic features in signals generated by the machine, such as mechanical vibrations or stator current signals (Abid et al., 2021; Garcia-Calva et al., 2022; Wang et al., 2022; Chen et al., 2024; Ziad et al., 2024). In particular, electrical faults represent 35%–40% of the failures in IMs (Gangsar and Tiwari, 2020), where stator windings failures are between 16% and 37% of failures that an IM can exhibit (Sheikh et al., 2022; Terron-Santiago et al., 2021; Niu et al., 2023), being the ITSC the most common failures in the stator windings.

One of the most employed techniques for fault detection in IMs is the Motor Current Signal Analysis (MCSA). This technique consists of acquiring the current signal from one or more phases of the IM stator and applying a specific method to extract the desired information for the detection and classification of faults. MCSA has demonstrated to be a practical approach for detecting electrical faults because it can be directly related to them (Gyftakis and Cardoso, 2021; Villalobos-Pina et al., 2024; Alloui et al., 2023). However, Gyftakis and Cardoso (Gyftakis and Cardoso, 2021) demonstrated the difficulty of detecting low-severity ITSC faults using traditional techniques. This issue is also exposed by Villalobos-Pina et al. (2024), who, through the implementation of conventional applications techniques based on MCSA, such as the Discrete Fourier Transform (DFT) and the Discrete Wavelet Transform (DWT) using Haar wavelet, found difficulties in reaching an accurate classification, leading to the integration of sophisticated techniques and methods such as a phasor analysis and a fuzzy logic system to handle this issue. Accordingly, other authors have explored the application of different signal processing methods in a non-conventional way, such as the well-known DWT, to extract features associated with the fault and then compute statistical parameters to discern among the possible faults (Sakhara et al., 2017; Almounajjed et al., 2021; Prakash et al., 2020; Susanta Ray and Dey, 2020). For example, Sakhara et al. (2017) report detecting ITSC faults with DWT at D3–D5 and A7 decomposition levels using a Daubechies wavelet; however, they do not provide a classification stage to evaluate the reported method. Alternatively, Almounajjed et al. (2021) compare techniques based on Fast-Fourier Transform (FFT) and multiresolution techniques based on DWT along with statistical parameters for detecting ITSC fault, identifying the ITSC fault in the detailed coefficients at level 7 using Daubechies wavelet and, consequently, reaching a better accuracy (96.72%) with 100% of mechanical load. In addition, techniques based on the FFT obtain spectrograms to detect the fault components (Ghanbari et al., 2022; Gyftakis, 2022; Hussain et al., 2021; Sakhara et al., 2017). Such as the case of Ghanbari et al. (2022) where the spectrograms, harmonics elimination, the histogram, and statistical indexes computation, such as the kurtosis and skewness, among other used techniques, are complemented for the ITSC fault detection. Unfortunately, Ghanbari et al. do not offer a quantitative analysis of the proposed method to confirm its effectiveness. Hussain et al. (2021) introduce a synergy between the FFT, Short-Time Fourier Transform (STFT), Continuous Wavelet Transform (CWT), and a model of deep learning to detect the ITSC fault, reaching up to 97.87% accuracy in simulated faulty signals. Other techniques, such as those applied by Sarkar et al. (2021) use the Principal Component Analysis (PCA) for detection of up to 1 Short-Circuited Turn (SCT) at no load and 30% of mechanical load condition, reaching 100% of accuracy. However, studies at higher mechanical load conditions are not included to prove the overall effectiveness. Mejia-Barron et al. (2019) applied brick-wall filters and Shannon Entropy (SE) to detect up to 10 SCTs with 98% of accuracy. Moreover, Bazan et al. (2019) introduce a method based on mutual information estimation with a Multilayer Perceptron (MLP) neural network to detect up to 3% of SCTs with an accuracy of 95%. While the aforementioned works report high accuracy rates, some of their limitations include the reliance on mechanical information to achieve the reported performance.

Beyond the feature extraction, the detection and classification of ITSC faults need classification algorithms to ensure the correct performance. So, artificial intelligence algorithms have been widely implemented due to their high reliability and accuracy. Algorithms such as Artificial Neural Network (ANN) (Bazan et al., 2019; Rajamany et al., 2019) and Convolutional Neural Network (CNN) (Jiménez-Guarneros et al., 2022; Susanta Ray and Dey, 2020; Shih et al., 2022; Faraj et al., 2023; Ziad et al., 2025) are the most used ones for this task. Unfortunately, these techniques typically require training with large datasets to identify patterns associated with specific faults. Additionally, such algorithms can be complex, computationally demanding, and often require specialized and costly hardware.

In addition, techniques based on histograms obtained from the stator current signals have proven to be effective in detecting faults in IMs, such as in detecting broken bars of rotors (Dias et al., 2020), bearing faults (Aviña-Corral et al., 2022; Tang et al., 2022), and other assessments in IMs (Dias et al., 2023; Glucina et al., 2023). One of the main advantages of this technique is its relative simplicity to implement, with minimal or no signal preprocessing required. However, despite the number of techniques applied today to the detection of ITSC faults in IMs, the development and application of different algorithms and methodologies are necessary, especially when the faults are incipient or when the mechanical load condition changes.

Addressing the issues previously mentioned, this paper presents a novel methodology based on the computation of the histogram from a CDF derived from a current stator signal where the fundamental frequency was removed to highlight the small components related to the ITSC faults; then, the CDF was decomposed into its sparse representation with the Orthogonal Matching Pursuit (OMP) algorithm to find similarities and differences across various fault classes. It is worth noting that the implementation of sparse representation has been applied in recent years to pattern recognition with excellent results (Morales-Perez et al., 2018; He et al., 2019; Qu et al., 2019), which outstanding dictionary-based performance motivates its utilization in machinery fault classification (Zhao et al., 2018). Although this approach was originally introduced in a different area (i.e., compressed sensing) (Rani et al., 2018; Zhang et al., 2015), its ability to reconstruct signals or images from specific and carefully chosen bases facilitates the identification of patterns (similarities or differences) to carry out the recognition task. In this regard, tools and algorithms from the literature, such as the OMP algorithm and the dictionary learning process developed by the K-Singular Value Decomposition (K-SVD) algorithm, are applied to store the features extracted from the CDFs obtained from current signals with the suppressed fundamental frequency, creating a novelty and well-structured methodology for ITSC fault detection, and

extending the integration of processing and classification methods in the ITSC faults detection area to elucidate the potential synergy of them. Through this approach, five levels of ITSC damage were detected under four different mechanical load conditions in a 2-hp IM, reaching accurate classifications without necessitating information about the load.

The innovations of the paper are listed as follows:

- New methodology for ITSC fault detection based on the CDF computation and the sparse representation with dictionary learning.
- Highlighting the ITSC faults into CDFs from the current signal with fundamental signal suppression using a sine/cosine filter.
- Reducing the number of dictionary atoms to just 35 significantly improves the OMP's performance for classification and detection applications compared with traditional overcomplete dictionaries containing more than 500 atoms, representing a reduction of over 90%.
- The training process can be developed using a small data set, achieving more than 98% accuracy.
- The developed training process generates dictionaries with sufficient information on damage levels and their behavior, ensuring that mechanical load does not affect the performance of the classification process.

2 Theoretical background

Electrical faults in IMs can be detected because the faults induce spurious components in the stator current spectra (Sheikh et al., 2022). In this context, MCSA can be effective for detection if the spurious signals into the current signal have sufficient amplitude. As with other faults, ITSC faults can distort the fundamental frequency component due to the presence of sines and cosines signals with a feature frequency (Niu et al., 2023), as presented below.

$$f_{itsc} = f_o\left[\frac{a}{p}(1-s) \pm b\right] \tag{1}$$

where f_o is the frequency of the fundamental sine signal from the power source, $a = \{1, 2, 3, \dots\}$ is an integer number, p is the pole-pair of the motor, s is the slip, and $b = \{1, 3, 5, \dots\}$ is an odd index. However, detecting these spurious frequencies is still a challenging task; in fact, the smaller the sine amplitude, the more difficult the detection. Therefore, MCSA technique usually requires a pre-processing technique in order to effectively extract the fault feature.

2.1 Fundamental signal suppression

The acquired motor current signal includes a fundamental component with a significant amplitude in contrast with any other harmonic component associated with the ones generated by the electrical faults from the stator, which mask the latter and complicate their detection. So, if the fundamental signal can be suppressed, the remaining signals can contain the spurious signals related to a stator fault with an amplitude that is easier to process.

To achieve this, it is necessary to generate a reference that effectively tracks the fundamental signal (both phase and amplitude). This can be reached by processing the target signal $\mathbf{x}$ to estimate the fundamental component. Accordingly, two sub-signals, denoted as $\mathbf{u}$ and $\mathbf{v}$, are generated based on the Discrete Sine and Cosine Transforms (Britanak et al., 2010; Morales-Perez et al., 2022), with their coefficients computed using the equations given below.

$$u[n] = \sum_{w=0}^{W-1} x[n+w]\ \frac{2}{W} sin\left[\frac{2\pi k(w+1)}{M}\right] \tag{2a}$$

$$v[n] = \sum_{w=0}^{W-1} x[n+w]\ \frac{2}{W} cos\left[\frac{2\pi k(w+1)}{M}\right] \tag{2b}$$

where $n = \{0, 1, 2, \dots, N-1\}$ is the $n-$th sample of a signal $\mathbf{x}$ of length N, W is the width of a window with a cycle of sine/cosine reference of $k-$th frequency, and M is the number of samples of the signal of interest in a second. Thus, W can be obtained as $W = \lceil M/k \rceil$; note that $k \equiv f$ (fundamental frequency) and $M \equiv f_s$ (sampling frequency). The arbitrary selection of the parameters defined above can result in the inefficiency of the filtering due to its direct relation to the suppression frequency and sampling rate.

This way, the amplitude of the fundamental signal can be obtained from the coefficients calculated in Equations 2a, b, applying Equation 3.

$$A[n] = \sqrt{u[n]^2 + v[n]^2} \tag{3}$$

Likewise, coefficients of an effective reference signal y can be generated according to Equation 4:

$$y[n] = \text{sign}\,(v[n])cos\,(\phi[n]) \tag{4}$$

where $y[n]$ is the n-th coefficient of $\mathbf{y}$, $\phi[n] = tan^{-1}(u[n]/v[n])$. Note that the resulting value of y[n] is between −1 and +1. This approach can suppress the fundamental signal by using:

$$r[n] = x[n] - A[n]y[n] \tag{5}$$

where $r[n]$ is the n-th coefficient of the remaining signal $\mathbf{r}$ with the fundamental suppressed.

An example of the fundamental signal suppression process is depicted in Figure 1. Note that the approach's effectiveness in correctly extracting the fundamental component must use a cycle of the fundamental signal; in this example, the suppression is adequate from 100 samples (see Figure 1a). A remaining signal can be obtained from Equation 5 (see the yellow plot in Figure 1a) that only contains information on the sidebands of the fundamental signal. This can be verified when obtaining the Power Spectral Density (PDS) (see Figure 1b), where the frequency components of the target signal $x[n]$ (blue plot) and the remaining signal $r[n]$ (red plot) are compared. As shown in Figure 1b, the filter can effectively suppress the primary frequency (fundamental sine signal from the power source) and does not affect other components significantly. In Figure 1b, the component f_a is

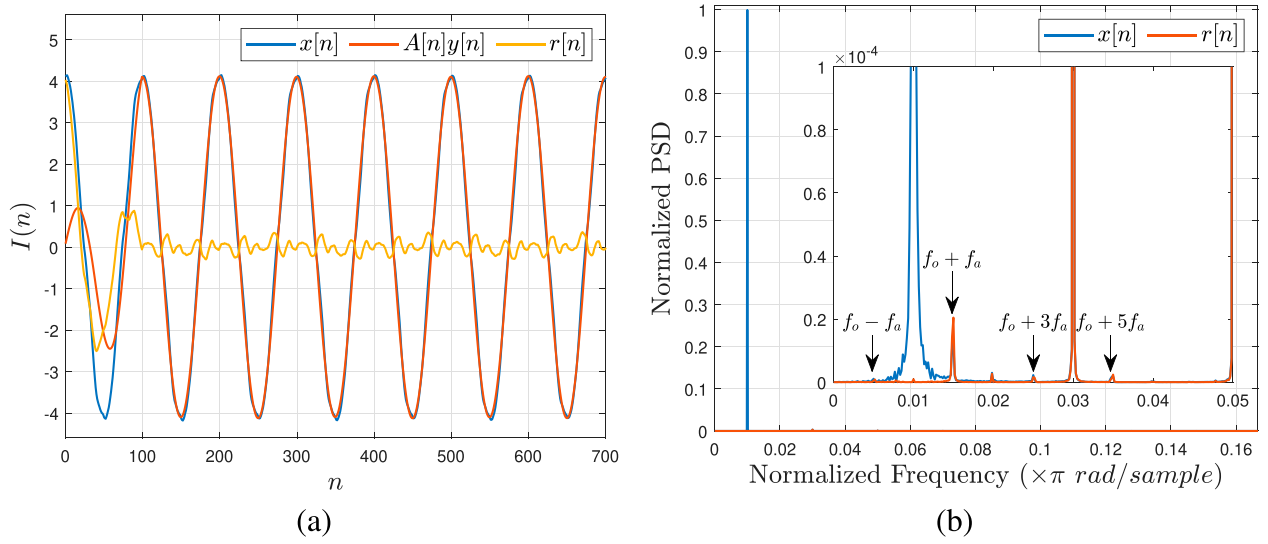

FIGURE 1
Example of the suppression process of the fundamental signal frequency component from a stator current signal: **(a)** time domain and **(b)** frequency domain.

the frequency of the ITSC fault sited to the sidebands of f_o in concordance with Equation 1, demonstrating the ITSC components preservation after of the filtering.

2.2 Sparse representation

Sparse representation involves decomposing a signal $\mathbf{x}$ into fundamental bases, represented as non-zeros coefficients $\alpha[m]$ (Rani et al., 2018; Zhang et al., 2015). This representation can be denoted by a linear combination as listed below:

$$x[n] = \sum_{m=1}^{M} D[n,m]\alpha[m] + r_s[n] \tag{6}$$

where $\mathbf{D} \in \mathbb{R}^{N\times M}$ is a dictionary with M fundamental signals or bases $\mathbf{b}_m$, $\alpha[m]$ is the m-th coefficient of a sparse vector $\alpha \in \mathbb{R}^{1\times M}$, and $r_s[n]$ is the n-th sample of a residual vector $\mathbf{r}_s \in \mathbb{R}^{N\times 1}$. It is import to note that $N \ll M$.

The representation Equation 6 can be considered sparse only if condition Equation 7 is met.

$$\min_{\alpha} \|x - D\alpha\|_2^2 \quad s.t. \quad \|\alpha\|_0 \leq K \ll N \tag{7}$$

where $\|\alpha\|_0$ is the ℓ_0 norm of the sparse vector α, and K is the sparsity. In other words, condition Equation 7 denotes that the sparse representation is a version of x with a few non-zeros coefficients due to $\tilde{\alpha} \forall \alpha_m \neq 0$ being a compressed version of x. On the other hand, as Equation 7 relies on an optimization problem, the proposing and application of diverse algorithms to obtain it is possible. Some algorithms for this purpose can be found in the literature (Zhang et al., 2015). This paper applies the OMP algorithm due to its fast convergence and relatively low complexity. Essentially, this algorithm determines the sparse representation of a signal by computing and selecting the best orthogonal projections between the signal and the given dictionary in an iterative manner. A pseudo-code of this is shown in Algorithm 1 (Morales-Perez et al., 2022).

```
Require: D and x.
Ensure: r_0 = x, D_0 = {}, U_0 = {}, and j = 0
  while (stop criterion is not met) do
    i = argmax_{m={1,...,M}} |⟨r_j, d_m⟩|
    U_j = [U_{j-1} ∪ i]
    D̃_j = [D̃_{j-1} | d_i]
    α̃_j = (D̃_j x^T)^{-1}
    r_j = x − D̃_j α̃_j
    j++
  end while
  return α̃_j, U_j, and r_j
```

Algorithm 1. Orthogonal Matching Pursuit.

Furthermore, the fidelity of the sparse representation does not only rely on the algorithm to obtain it, the determination of the dictionaries is also a crucial task, being necessary the study the types of signal to be represented. This challenge has led to development of methods to construct them effectively, e.g., the construction of dictionaries from mathematical transforms is recommended if the signals are periodic and well-determined in shape, phase, and amplitude (Morales-Perez et al., 2022). A Different process is recommended for signals without a defined shape, containing very specific features, or when the representation from space transformation is not feasible (Gangeh et al., 2015). The latter scenario can be addressed by applying algorithms like the K-SVD introduced by Aharon et al. (2006), which is utilized in this paper due to its effectiveness in generating dictionary atoms.

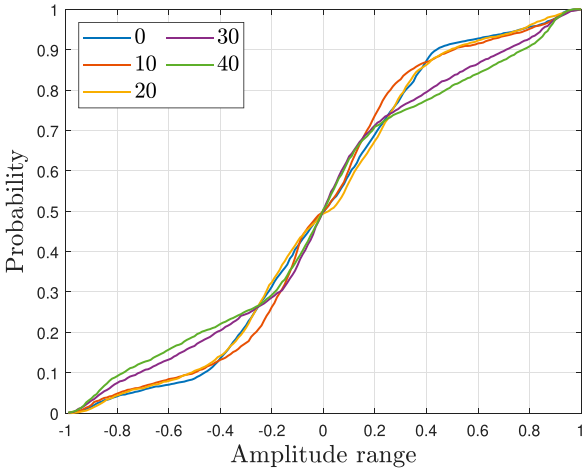

FIGURE 2
Example of CDFs obtained from a remaining signal **r** with an ITSC fault. 0, 10, 20, 30, and 40 are the number of short-circuited turns in the stator.

3 Methodology

The feature extraction of a specific failure into the stator current signal can be a challenge. Therefore, this paper proposes a methodology to detect ITSC faults by processing the stator current using cumulative histograms and sparse representation.

The first stage consists of removing the principal component of the stator current signal. This stage is developed for extracting and highlighting the elements related to the fault for detection. This process is conducted as.

1. Obtain $u[n]$ and $v[n]$, applying Equations 2a, b respectively, selecting the length of a window W for a cycle of the fundamental signal to be suppressed.
2. Then, compute the amplitude of the fundamental signal using Equation 3.
3. Next, generate a reference signal by applying Equation 4.
4. Finally, suppress the fundamental signal using the reference generated and the previously estimated, as specified in Equation 5. The remaining signal $r[n]$ will used for the next stage.

The obtaining of the cumulative histogram is the second stage. Cumulative histograms are histograms obtained from the CDF of a data set $X = \{x[0], x[1], \ldots, x[n]\} \forall\, x[n] \in \mathbb{R}$ (Leon-Garcia, 2017). In this way, the CDF is defined in Equation 8.

$$h_c(x) = P(X \leq x) \tag{8}$$

where $P(X \leq x)$ is a function that fits $X \leq x$. Following the above, the CDF of r[n] is obtained to get a pattern that includes only the information of the possible faults (see Figure 2), with no regard for the phase shift of the acquired signal.

From Figure 2, the differences from CDFs with 0, 10, 20, 30, and 40 short circuit turns in the stator can be observed. The distortion of these CDFs is caused by the fault features, allowing distinction among them.

The following stages consist of developing the classification process. First and foremost, a training process to generate the necessary information for fault detection based on sparse representation must be developed. Then, the classification process can be executed to identify the possible fault of the stator motor. These processes are described in detail in the following sub-section.

3.1 Training process

This process consists of obtaining the necessary dictionaries for classifying the faults employing a training algorithm, which is, in other words, the well-named dictionary learning process. The K-SVD algorithm is used for this purpose, employing a training set of signals (or, in this case, histograms) that share the same features. In line with the standard training stage, the proposed approach employs K-SVD exclusively for dictionary learning. Once the dictionary attains the desired quality, the algorithm is no longer required. In this sense, the algorithm will find the training set's features and adjust the dictionary's atoms to represent each reference in an effective sparse representation. The process is iterative, and the algorithm's convergence depends on the complexity of the features extracted from the training set. Therefore, a dictionary must be generated for each fault so the OMP algorithm can distinguish them. The pseudocode described in Algorithm 2 summarizes the applied K-SVD algorithm.

```
Require: D_0, X, K, and M
for k = 1 to K do
  Use the OMP algorithm to obtain α
  for j = 1 to M do
    ω = {i ∈ 1,2,...,M} s.t. α_k[j,i] ≠ 0
    α_ω[j,ω] = 0
    R = X_ω − D_k α_ω
    UΔV = SVD(R)
    d_j ∈ D_k = u_1
    α_ω[j,ω] = v_1 Δ(1,1)
  end for
end for
return D_k
```

Algorithm 2. K-Singular Value Decomposition.

It is important to note that Algorithm 2 requires the K and M values to function, where K is the number of iterations to adjust the dictionary and the M is the number of atoms of the dictionary. $\mathbf{D}_0$ and $\mathbf{X}$ are the initial dictionary and the training set, respectively. Finally, the algorithm returns the trained dictionary $\mathbf{D}_k$, used in the next and last stages.

3.2 Classification process

Once the dictionaries have been trained, the classification process can be carried out. The process involves the introduction of the CDF obtained in the above stages to the OMP algorithm (see

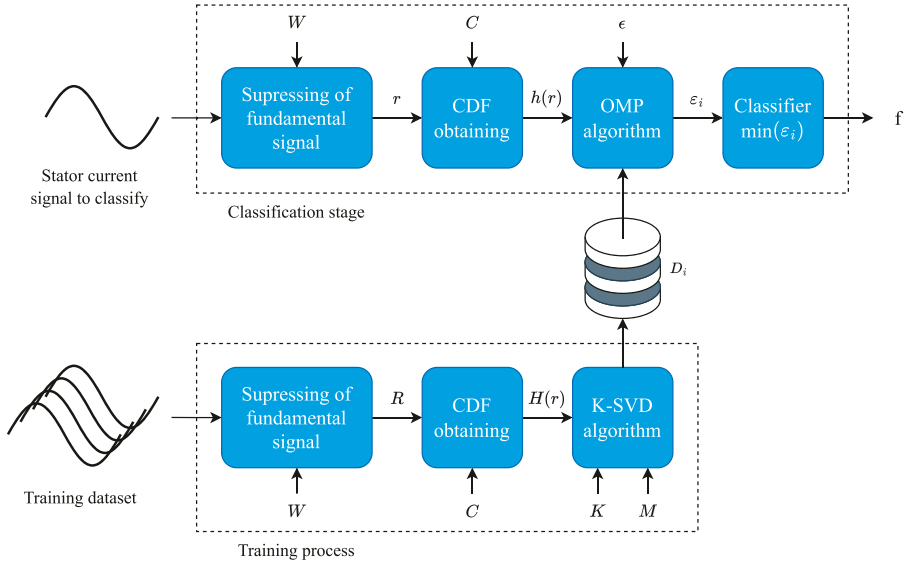

FIGURE 3
General block diagram of the proposed methodology.

Algorithm 1). For this purpose, the stop criterion selected for the OMP algorithm is the maximum reconstruction error Equation 9. In this manner, the sparse representation is expected to be better with only the dictionary that contains the features that match the features of the CDF, reducing the reconstruction error with this specific dictionary. Accordingly, the reconstruction error metric is selected because it aligns with the underlying least-squares formulation of sparse representation, enabling the evaluation of the energy contributed by the selected atoms rather than merely assessing the signal shape. (Morales-Perez et al., 2018; Zhao et al., 2018).

$$\varepsilon \leq \epsilon \quad s.t. \quad \varepsilon = \frac{\|\mathbf{r}\|_2}{\|\mathbf{x}\|_2} \tag{9}$$

where ϵ is the maximum permissible reconstruction error, ε is the actual reconstruction error reached by the OMP, and $\|\bullet\|_2$ is the ℓ_2 norm. It is important to note that $\mathbf{x} \leftarrow h_c$ is in the OMP algorithm. In this way, each sparse representation obtained with each dictionary $\mathbf{D}_i$ returns a reconstruction error ε_i.

So, the classification is reached by selecting the minimum error ε_i, indicating the fault features contained in the CDF detected in a dictionary by the OMP algorithm.

$$\mathrm{f} = \min_{i=\{1,\ldots,P\}} (\varepsilon_i) \tag{10}$$

where f is the index of the featured fault, and P is the number of faults to detect. Both processes, training and classification, are summarized in the general block diagram depicted in Figure 3.

4 Experimental setup

The current signals used to develop and validate the proposal were acquired by using the experimental setup illustrated in Figure 4. This test bench was implemented to replicate well-established configurations reported in the literature and to comply with the recommended, widely adopted test conditions. Table 1 shows the information and the main characteristics of the principal equipment and the devices used in the experimental setup. In this regard, the induction motor was modified to simulate the ITSC with the following severities: 0, 10, 20, 30, and 40 SCTs in a single-phase winding, where the total of turns is 141 turns. The mechanical loads were induced with the dynamometer to obtain the following load levels: 0%, 33.3%, 66.6%, and 100% of its nominal mechanical load.

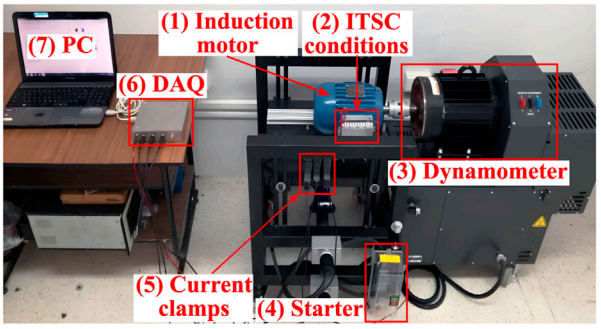

FIGURE 4
Experimental setup.

The current signals were acquired by the current clamp connected to the data acquisition system board, configured with a sampling frequency of 6 kHz. A data set was created with 20 tests per severity and load condition with a duration of 3.5 s (obtaining 21,000 samples) only in order to minimize the physical damage that can be provoked to the stator with the simulated faults. Hence, a total of 400 signals were acquired in the IM steady states conditions and stored in the database proprietary of the laboratory of Sistemas

TABLE 1 Main equipment and devices used in the experimental setup.

Equipment/Device	Brand	Model	Main characteristics
(1) Induction Motor	WEG	218ET3EM145TW	Three-phase, 2 hp, 220 V, 60 Hz
(2) ITSC conditions	–	–	0, 10, 20, 30, and 40 SCT.
(3) Dynamometer	Lab-Volt	8,540	Four-quadrant, three-phase, 12 A, speed range 0–3,600 rpm, nominal torque 0–12.18 Nm
(4) Starter	Siemens	3RT2018-1AN61	Three-phase, 200–220 V @ 60 Hz, AC-3e/AC-3, 16 A, 7.5 kW/400 V
(5) Current clamps	Fluke	i200s	CAT III 600 V, dual range 20/200 A, output 10/100 mV/A
(6) DAQ	National Instruments	USB-6211	8 differential or 16 single-ended inputs, 16-bit resolution, 250 kS/s
(7) PC	Dell	G15	16 GB of RAM, 512 GB SSD NVMe, Intel Core i5 @ 2.6 GHz

Dinámicos, Facultad de Ingeniería, Universidad Autónoma de Querétaro (UAQ), Campus San Juan del Río, which can be accessed by formal request and upon signing an agreement for academic research purposes.

5 Experimental results

Once all current signals were acquired in the steady state of the IM, each acquired signal was segmented into seven parts, with each part containing 0.5 s of information. According to the preliminary testing, 0.5 s is enough time in order to conserve the features related to ITSC in the current signal and reduce the amount of data for analysis and, consequently, the computational time consumption. In this way, the created data set for this paper is 2,800 segments of the current signal in a steady state of IM for all conditions. Following the proposed methodology, the suppression of the fundamental signal is firstly conducted using the procedure described above to highlight the presence of the components related to the ITSC faults; otherwise, the fundamental signal, being of relatively larger amplitude, tends to conceal them and make their detection more difficult. Then, the CDF is computed to obtain a defined pattern regardless of the phase of the spurious component in the preprocessed signal. So, to detect these patterns that may show slight changes between them, the dictionary training process has to be carried out.

To avoid bias, this process was validated using a 5-fold cross-validation as recommended in the literature (Marcot and Hanea, 2021; Morales-Perez et al., 2018). This validation consists of randomly selecting the signals used for the training process; the remaining is used for the validation process. The latter was repeated five times. The CDFs were obtained as explained in the methodology section; each signal segment in the steady state of 0.5 s length was normalized to an amplitude of ± 1 to ensure all signals are within the same amplitude range. Then, they were converted into CDFs with 200 classes (steps of 0.01), enough for the development of the classification, accordingly with the preliminary tests. For each condition, 140 CDFs were obtained, with 40 randomly selected to train the dictionaries and 100 for testing. The dictionaries for training were created with $M = 35$ atoms: the first atom as ℓ_2 normalized CDF from a sine signal of 2 Hz and the other 34 atoms as a constant of $1/\sqrt{200}$. This way, the K-SVD algorithm starts from a specific base and adjusts the atoms from a principal feature (first atom). Thereby, the remaining features are saved into the other atoms (initially constants), ensuring the extraction of significant features according to the fault severities and avoiding the over-training of atoms.

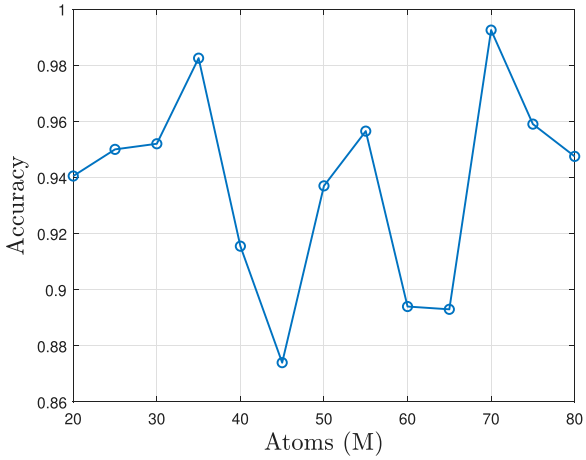

FIGURE 5
Average accuracies reached by different values of *M*.

The selection of the number of atoms was based on the results of the tests resumed in the plot depicted in Figure 5, which indicated that the dictionaries with more than 35 atoms ($M > 35$) did not achieve significant improvements and increase the computational time-consumption. Even though the literature precise that dictionaries trained with $K = 35$ reach an acceptable performance for specific applications (Morales-Perez et al., 2018), the number of iterations for the training process was configured to $K = \{50, 60, 70, 80, 90, 100\}$ to research the effectiveness of the trained dictionaries.

Also, the OMP was configured to reach a maximum reconstruction error of $\epsilon = 0.001$ due to the minor differences in the CDFs for closely faults in terms of severity. So, higher values of ϵ can decrease the method's effectiveness. An example of the reconstruction from the sparse representation obtained through the OMP algorithm is depicted in Figure 6. This example presents a CDF reconstructed with different dictionaries (as proposed in this work), trained with 10, 20, 30, and 40 SCTs. It may be noticed that the reconstruction (red plot) has discrepancies compared to the original CDF (blue plot), and these discrepancies increase if the employed dictionary does not match the group of the

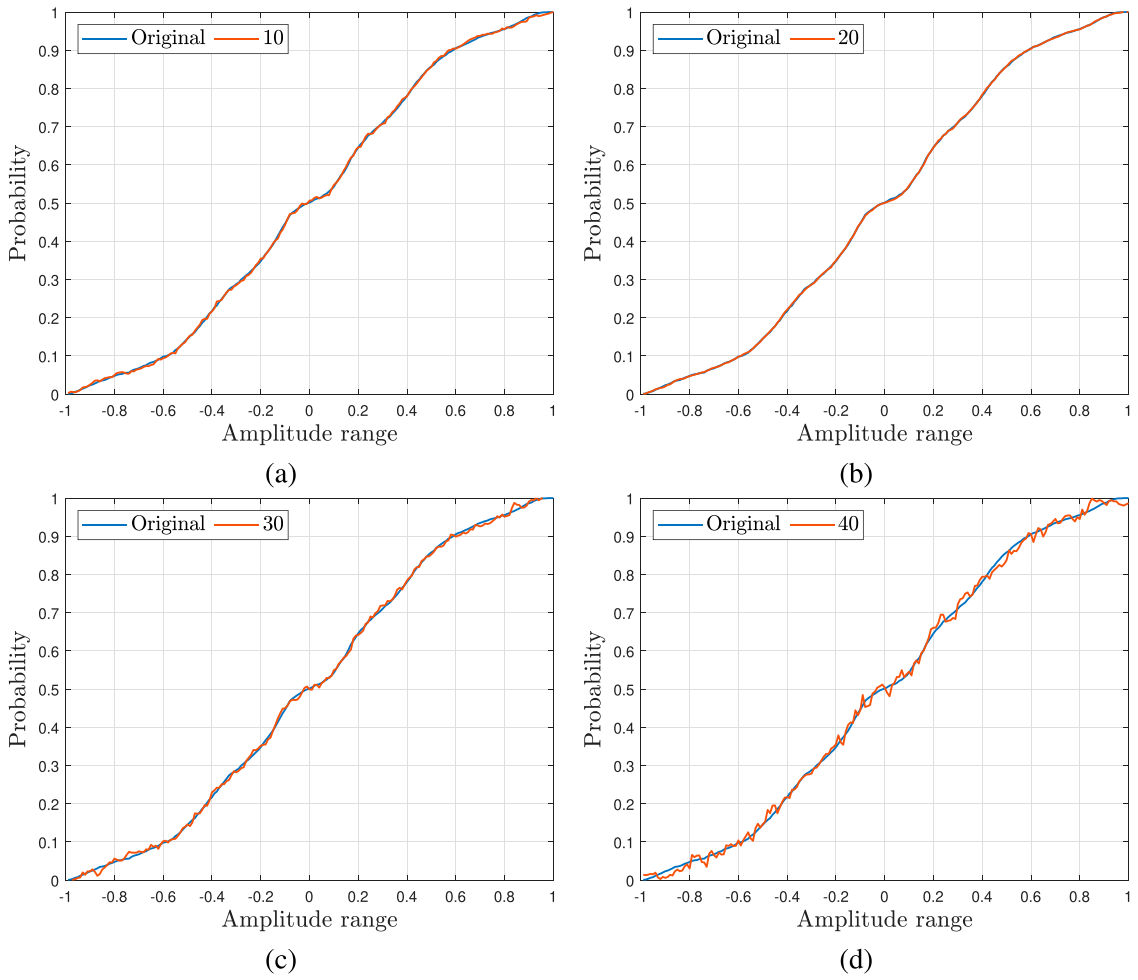

FIGURE 6
Example of reconstruction from the sparse representation obtained with the OMP algorithm and the trained dictionaries: **(a)** 10 SCT, **(b)** 20 SCT, **(c)** 30 SCT, and **(d)** 40 SCT.

reconstructed CDF (see the plot in Figure 6d). This occurs because the dictionary does not have enough features in its atoms to offer an effective sparse representation and reconstruction; consequently, the OMP algorithm uses all the available dictionary information to represent the input CDF, resulting in a CDF with pronounced differences over the original. This is not the case when the dictionary has enough features in its atoms. In this way, it is notable that the fault contained in the reconstructed CDF is 20 SCTs, which best fits with the original CDF (see the plot in Figure 6b). Reconstruction errors ε_i obtained from these tests were 0.0064, 0.0010, 0.0088, and 0.0168, concluding that the best dictionary for this reconstruction is the one trained with 20 SCT ($\varepsilon = 0.001$), indicating a correct classification from Equation 10. Table 2 presents the overall results of the test development with different K parameters for the training process.

The accuracy per the condition of the tests was calculated using Equation 11.

$$ACC = \text{mean}(A_i) \pm \text{std}(A_i) \quad s.t. \quad A_i = \frac{N_{TP}}{N_t} \times 100\% \qquad (11)$$

where A_i is the i-th accuracy of each fold cross-validation, N_{TP} is the number of true positives, and N_t is the number of total samples of the specific condition. The global accuracies per K is: 96.63% ± 2.218, 97.77% ± 1.92475, 97.8% ± 1.9833, 97.96% ± 2.0063, 97.6% ± 2.0106, and 98.24% ± 1.8479; for K50, K60, K70, K80, K90, and K100, respectively.

As shown in Table 2, the best performance is reached with a trained dictionary with 60 iterations (K60). Parameters exceeding 60 do not show a significant increase in the global accuracy of the test; indeed, a number greater than 60 iterations for this application results merely in minor adjustments to the atoms, implying more time consumption with very small changes in the behavior and effectiveness. Therefore, 60 iterations is selected in this work, which is enough to reach a practical accuracy (~ 98%) and distinguish the severity of the fault regardless of mechanical load. In addition, it is worth noting that the threshold of maximum reconstruction error $\epsilon = 0.001$ underscores the methodology's capacity to discern between faults, even those with minimal differences, a noteworthy challenge in this field.

Furthermore, additional tests were developed to verify the effectiveness of the methodology's proposed workflow. These

TABLE 2 Accuracy results with different training iterations parameter (K).

Load	Severity (SCT)	Accuracy [ACC (%)]					
		K50	K60	K70	K80	K90	K100
0.00%	0	89.200 ± 7.085	93.000 ± 3.391	89.000 ± 8.216	93.400 ± 5.459	89.600 ± 8.503	88.800 ± 11.563
	10	90.400 ± 6.025	95.400 ± 2.966	97.000 ± 2.449	94.400 ± 5.983	96.000 ± 2.121	97.400 ± 3.130
	20	92.800 ± 3.962	95.000 ± 4.000	95.400 ± 1.517	94.600 ± 7.893	97.400 ± 1.949	97.400 ± 2.881
	30	97.200 ± 2.168	98.400 ± 2.074	97.800 ± 2.280	98.000 ± 1.871	93.000 ± 5.788	99.000 ± 0.707
	40	96.000 ± 4.528	95.800 ± 4.919	97.600 ± 3.362	98.800 ± 1.304	97.400 ± 3.782	99.200 ± 0.837
33.33%	0	86.000 ± 4.950	94.800 ± 2.387	96.400 ± 2.608	96.000 ± 1.000	97.600 ± 2.074	95.400 ± 3.647
	10	95.400 ± 0.894	96.600 ± 1.817	96.800 ± 3.564	97.000 ± 2.550	94.600 ± 3.975	98.800 ± 1.304
	20	99.400 ± 1.342	97.800 ± 2.950	99.800 ± 0.447	99.000 ± 1.732	99.800 ± 0.447	99.800 ± 0.447
	30	99.400 ± 0.894	99.600 ± 0.548	99.000 ± 1.414	100.000 ± 0.000	99.400 ± 0.548	97.800 ± 4.382
	40	98.600 ± 1.673	99.200 ± 1.304	99.800 ± 0.447	99.800 ± 0.447	99.200 ± 1.789	99.600 ± 0.548
66.66%	0	97.400 ± 2.191	98.200 ± 2.683	94.200 ± 5.119	97.400 ± 1.949	97.400 ± 1.949	97.600 ± 3.286
	10	99.000 ± 0.707	99.200 ± 0.837	99.200 ± 0.837	97.800 ± 2.950	99.000 ± 0.707	99.200 ± 0.447
	20	97.000 ± 2.550	98.600 ± 1.140	99.600 ± 0.548	97.600 ± 3.362	97.000 ± 1.581	98.400 ± 0.894
	30	99.200 ± 0.447	99.200 ± 0.837	99.400 ± 0.548	99.000 ± 0.000	98.800 ± 1.095	99.200 ± 0.837
	40	98.000 ± 1.871	98.400 ± 2.510	99.000 ± 0.000	98.400 ± 1.342	98.200 ± 2.387	99.000 ± 0.707
100.00%	0	98.800 ± 0.837	97.600 ± 1.517	96.800 ± 4.970	99.200 ± 0.837	97.600 ± 1.517	98.400 ± 0.894
	10	99.400 ± 1.342	99.800 ± 0.447	99.400 ± 0.894	100.000 ± 0.000	100.000 ± 0.000	100.000 ± 0.000
	20	100.000 ± 0.000	100.000 ± 0.000	100.000 ± 0.000	99.800 ± 0.447	100.000 ± 0.000	100.000 ± 0.000
	30	100.000 ± 0.000	100.000 ± 0.000	100.000 ± 0.000	100.000 ± 0.000	100.000 ± 0.000	100.000 ± 0.000
	40	99.400 ± 0.894	98.800 ± 2.168	99.800 ± 0.447	99.000 ± 1.000	100.000 ± 0.000	99.800 ± 0.447

tests, A, B, and C, involve an ablation analysis and evaluation of the results. Test A consists of developing the methodology presented in this work; Test B is a similar development to the proposed method, but the dictionary initialization is random; and finally, Test C generates dictionaries in the time domain with the dictionary randomly initialized. Examples of confusion matrices are depicted in Figure 7; note the mistakes increase from the classifier between test A and test B, especially at no mechanical load and low damage levels, and the lousy classification in test C. Global accuracies are shown in Table 3. As expected, the best results are with the CDFs, highlighting the improvement of the accuracy of the dictionaries that are initialized as previously exposed in contrast with the random initialization. Otherwise, the accuracies reached with dictionaries trained in the time domain are very low due to the phase shift during the acquired stage, requiring the increasing of the numbers of atoms (M) to manage this issue, reaching the inequality $M \gg N$ and increase the time-consumption noticeably during the training process.

It should be pointed out that the required length of the signal to reach the fault detection is 0.5 s, which decreases the number of samples (to 3,000 samples) that need to be processed. This is in contrast to other methodologies that require 1 s or longer to reach comparable performance (Cardenas-Cornejo et al., 2023; Mejia-Barron et al., 2019; Chen et al., 2023; Jiménez-Guarneros et al., 2022).

According to the theory study of the technique's sparse representation and classification purpose, the classification is possible as the atoms of the applied dictionaries have enough information; that is, the sparse representation is obtained with high-quality dictionaries. To evaluate the reconstruction performance and quality of the trained dictionaries, the logarithm of the Root Mean Square Error (RMSE) was computed (Sadeghi et al., 2013). This measure is defined in Equation 12:

$$E_{log} = log_{10}\left(\frac{\|\mathbf{X} - \mathbf{D}\alpha\|_F}{nL}\right) \tag{12}$$

where $\mathbf{X}$ is the set of used signals (CDFs in this paper), $\mathbf{D}$ is the testing dictionary, α is the sparse representation of the set of signals $\mathbf{X}$ for the $\mathbf{D}$ dictionary, n is the number of samples in each signal, L is the number of signals into the set $\mathbf{X}$, and $\|\bullet\|_F$ is the Forbenius norm.

Measuring results are depicted in Figure 8. Note the highlighted differences between the results in dictionaries trained current signal in the time domain (Figure 8a) and the trained with proposed CDFs (Figure 8b). The quality of the dictionaries increases as the E_{log} is more negative; that is to say, the small squares in the plot acquire a dark blue color. In this regard, a remarked diagonal appears in the

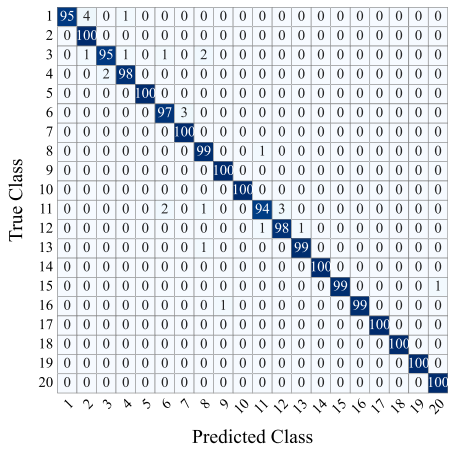

(a)

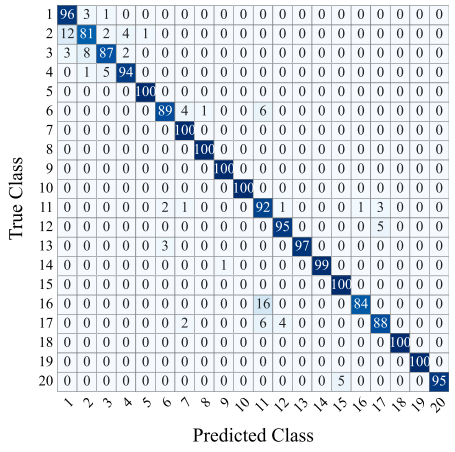

(b)

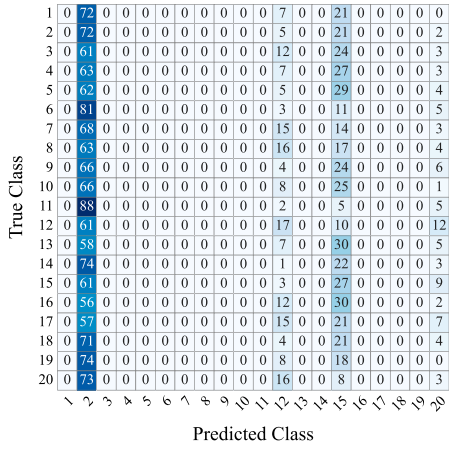

(c)

FIGURE 7
Example confusion matrices from ablation analysis: **(a)** Test A; **(b)** Test B; and **(c)** Test C. [Labels 1, 2, 3, 4, and 5 correspond to 0, 10, 20, 30, and 40 SCTs at 0% of mechanical load, respectively; 6–10 correspond to 0–40 at 33.33%; labels 11–15 correspond to 0–40 at 66.66%; and 16–20 correspond to 16–20 at 100%].

graph of the measuring of the dictionaries trained with the proposed CDFs, indicating the dictionary that belongs to the same class of the

TABLE 3 Global average results of the additional tests.

K (M = 35)	Accuracy [ACC (%)]		
	Test A	Test B	Test C
50	96.05	93.00	4.60
60	98.10	94.40	3.70
70	98.65	94.80	5.00
80	98.10	94.45	4.40
90	98.20	94.60	5.95
100	98.20	95.40	3.55

CDF (or signal) has a high probability of detecting it (or reconstructed it), giving the high accuracy rate above demonstrated. This is not the case with the dictionaries trained with current signals in the time domain, where the diagonal is diffused. These results demonstrate the superiority and the high performance of the dictionaries trained with the proposed CDFs, with only 35 atoms in contrast with the suggested in the literature (Rani et al., 2018; Zhang et al., 2015) ($N \ll M$), at least in this type of application.

6 Discussion

Table 4 provides a comparative analysis of the proposed methodology against other works reported in the literature. As can be observed, the proposed method shows accuracy relative to other works (Bazan et al., 2019; Cardenas-Cornejo et al., 2023; Chen et al., 2023) enabling the detection fault of faults as minimal as 10 SCTs, which constitute 7% of the total turns in the stator winding. Although other papers report the identification of more incipient faults (Bazan et al., 2019; Cardenas-Cornejo et al., 2023), their accuracies are around 83%, which is more than 10% lower than the accuracy reported in this work. Even though there are works with comparable accuracy rates, e.g., (Mejia-Barron et al., 2019), they are susceptible to mechanical load, a challenge in most work in this field. In contrast, this work can distinguish the faults regardless of the mechanical load, unlike (Bazan et al., 2019; Cardenas-Cornejo et al., 2023; Chen et al., 2023), which requires testing under specific load conditions and necessitates knowledge of the load for accurate detection. On the contrary, the proposed method only needs the CDF input, which in turn identifies the fault level regardless of the applied mechanical load. Another advantage of the proposed methodology is the use of few atoms in the dictionaries, in contrast with traditional sparse representation methodologies that need more atoms than their number of samples (Morales-Perez et al., 2018), reducing the time consumption and increasing the performance efficiency.

Furthermore, ANNs and CNNs have demonstrated exceptional performances in classification applications. However, these architectures usually need a considerable data set size to reach their characteristic classification rates and the application of specific hardware to develop their training stages. Table 5 shows the classification test results with some artificial intelligence

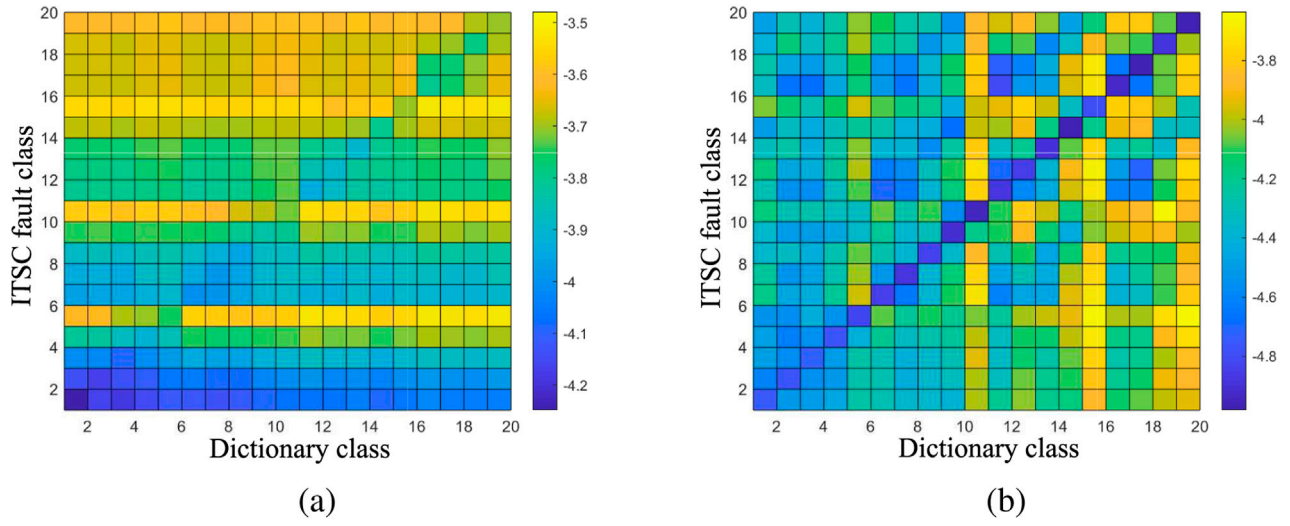

FIGURE 8
Graphs of measuring the quality of the dictionary (E_{log}): **(a)** dictionaries trained with current signals in the time-domain; **(b)** dictionaries trained with CDFs with fundamental signal suppressed.

TABLE 4 Comparison between the proposed methodology and other methods for ITSC fault detection in the literature.

Work	Techniques	Type of signal (domain)	Accuracy	Mechanical load	Severities (SCT)	Load info
Mejia-Barron et al. (2019)	1. Brick-wall band-pass FIR filters for features extraction. 2. Shannon Entropy index for fault indicator. 3. Fuzzy Logic system as a classifier	Current (time)	98%	0, 33.33, 66.66, and 100%	0, 10, 20, 30, and 40	Necessary
Bazan et al. (2019)	1. Delayed Mutual Information algorithm as feature extraction. 2. Multilayer Perceptron ANN as a classifier	Current (time)	83%	(0.9:0.4:9.3) Nm	1, 3, 5, and 10%	Necessary
Cardenas-Cornejo et al. (2023)	1. Quaternions and statistical indexes as feature extraction. 2. Decision tree models as a classifier	Current (time)	83.33%	No load	0, 6, 12, 18, and 24	Necessary
Chen et al. (2023)	1. Sliding-Average Filter as a pre-processing stage. 2. Envelope extraction and Gaussian Window Weighting as feature extraction. 3. SVM as a classifier	Current (time)	96%	0, 0.52, and 1.04 Nm	0, 2, and 6	Necessary
This work	1. Sine-Cosine filter to suppress the fundamental signal. 2. CDF histograms as a fault indicator. 3. OMP algorithm as a classifier	Current (time)	98%	0, 33.33, 66.66, and 100%	0, 10, 20, 30, and 40	Unnecessary

algorithms under the same training condition of the proposed methodology.

MLP implemented architecture is a small ANN and configured to be compatible with the input CDFs and the out classes, for which an accuracy of 90.33% is reached after 3,000 epochs. The small CNN 1D architecture was taken from (Jiménez-Guarneros et al., 2022) and modified to preserve compatibility with the proposed CDF, reaching 75.15% of accuracy after the 3,000 epochs. Finally, implementing a conventional ResNet 1D reaches 95.94% after the 120 epochs. In all cases, the training set contained 800 CDFs (40 per class), and the testing set had 2000 CDFs, the same condition under which the proposed methodology is presented. However, the proposed classification process performed better, reaching 98.24% with 100 iterations and surpassing the ResNet 1D accuracy at 50 iterations (96.63%).

TABLE 5 Comparison results of classification test with artificial intelligence algorithms and the proposed classification.

Metric	MLP	CNN 1D	RestNet 1D	Proposal
Average Accuracy	90.33%	75.18%	95.94%	98.24%

In addition, advantages such as the intrinsic noise tolerant feature of the OMP algorithm (Morales-Perez et al., 2022; Wang, 2015; Wu et al., 2013) and the hardware-based architectures available in the literature (Ge et al., 2019; Roy et al., 2019; Li et al., 2021; Roy et al., 2021) make this approach suitable for real-time applications in industrial environments.

7 Conclusion

A novel methodology based on obtaining the CDF of the current stator signal with fundamental signal suppression and sparse representation was presented in this work for ITSC fault detection. By suppressing the fundamental signal, the components of the ITSC faults are highlighted, allowing a more effective detection. This is evidenced by the 98% classification rate achieved. The effectiveness of the proposed method is due to the OMP algorithm, which facilitates an efficient reconstruction with the sparse reconstruction obtained from dictionaries trained with specific faults, resulting in a lower reconstruction error for dictionaries that contain the features of the same fault. Additionally, the algorithm demonstrates the capacity to discern between all the treated faults (0, 10, 20, 30, and 40 SCTs), even if these have slight differences. This is supported by the maximum reconstruction error $\epsilon = 0.001$ used and recommended in this work. Another noteworthy aspect is that the training process for the dictionaries with the K-SVD algorithm does not require more than $K = 60$ iterations. Finally, an outstanding feature of the proposed method is that faults are classified without regard to the mechanical load (0, 33.33, 66.66, and 100%); that is, the classifier does not need additional information about the current mechanical load to operate effectively. In addition, dictionary dimension reduction, from an overcomplete dictionary (usually, more than $M = 500$ atoms reported in the literature) to $M = 35$, represents a considerable reduction of workload. This feature enables the proposal to be used in various industrial applications. According to the testing results, the extension of this research to incipient faults (5 SCTs) will be explored in future work, including the integration of deep learning models, extension to another motor type, other fault types, such as bearing faults, and multiple faults. Also, implementing this method in embedded systems for real-time applications is considered a viable possibility. In addition, despite the favorable results, future studies will be considered to enhance its robustness and resolve possible limitations of time-varying regimens, other percentages of mechanical load, dynamic mechanical profiles, and perturbations in the power line network, which could introduce new behaviors in CDFs.

Data availability statement

The datasets presented in this article are not readily available because Institutional restrictions. Requests to access the datasets should be directed to martin.valtierra@enap-rg.org.

Author contributions

CM-P: Conceptualization, Data curation, Formal Analysis, Investigation, Software, Validation, Writing – original draft. JA-S: Conceptualization, Data curation, Methodology, Resources, Writing – original draft. JR-M: Conceptualization, Data curation, Methodology, Resources, Writing – original draft. DG-L: Formal Analysis, Methodology, Resources, Software, Validation, Writing – original draft. MV-R: Conceptualization, Data curation, Formal Analysis, Funding acquisition, Investigation, Methodology, Project administration, Resources, Software, Supervision, Writing – original draft, Writing – review and editing.

Funding

The author(s) declared that financial support was not received for this work and/or its publication.

Acknowledgements

The author, CM-P, thanks the "Secretaría de Ciencias, Humanidades, Tecnología e Innovación (SECIHTI)–México" for supporting a postdoctoral stay at the "Universidad Autonoma de Queretaro (UAQ)–México". The authors would like to thank the (SECIHTI)–México and the "Sistema Nacional de Investigadoras e Investigadores (SNII, SECIHTI)–México" for their support in this research.

Conflict of interest

The author(s) declared that this work was conducted in the absence of any commercial or financial relationships that could be construed as a potential conflict of interest.

The authors MV-R, JA-S declared that they were an editorial board member of Frontiers at the time of submission. This had no impact on the peer review process and the final decision.

Generative AI statement

The author(s) declared that generative AI was not used in the creation of this manuscript.

Any alternative text (alt text) provided alongside figures in this article has been generated by Frontiers with the support of artificial intelligence and reasonable efforts have been made to ensure accuracy, including review by the authors wherever possible. If you identify any issues, please contact us.

Publisher's note

All claims expressed in this article are solely those of the authors and do not necessarily represent those of their affiliated organizations, or those of the publisher, the editors and the reviewers. Any product that may be evaluated in this article, or claim that may be made by its manufacturer, is not guaranteed or endorsed by the publisher.

References

Abid, A., Khan, M. T., and Iqbal, J. (2021). A review on fault detection and diagnosis techniques: basics and beyond. *Artif. Intell. Rev.* 54, 3639–3664. doi:10.1007/s10462-020-09934-2

Aharon, M., Elad, M., and Bruckstein, A. (2006). K-svd: an algorithm for designing overcomplete dictionaries for sparse representation. *IEEE Trans. Signal Process.* 54, 4311–4322. doi:10.1109/TSP.2006.881199

Alloui, A., Laadjal, K., Sahraoui, M., and Marques Cardoso, A. J. (2023). Online interturn short-circuit fault diagnosis in induction motors operating under unbalanced supply voltage and load variations, using the stlsp technique. *IEEE Trans. Industrial Electron.* 70, 3080–3089. doi:10.1109/TIE.2022.3172751

Almounajjed, A., Sahoo, A. K., and Kumar, M. K. (2021). Diagnosis of stator fault severity in induction motor based on discrete wavelet analysis. *Measurement* 182, 109780. doi:10.1016/j.measurement.2021.109780

Aviña-Corral, V., de Jesus Rangel-Magdaleno, J., Peregrina-Barreto, H., and Ramirez-Cortes, J. M. (2022). Bearing fault detection in asd-powered induction machine using modwt and image edge detection. *IEEE Access* 10, 24181–24193. doi:10.1109/ACCESS.2022.3154410

Bazan, G. H., Scalassara, P. R., Endo, W., Goedtel, A., Palácios, R. H. C., and Godoy, W. F. (2019). Stator short-circuit diagnosis in induction motors using mutual information and intelligent systems. *IEEE Trans. Industrial Electron.* 66, 3237–3246. doi:10.1109/TIE.2018.2840983

Britanak, V., Yip, P. C., and Rao, K. R. (2010). *Discrete cosine and sine transforms: general properties, fast algorithms and integer approximations*. Elsevier.

Cardenas-Cornejo, J.-J., Ibarra-Manzano, M.-A., González-Parada, A., Castro-Sanchez, R., and Almanza-Ojeda, D.-L. (2023). Classification of inter-turn short-circuit faults in induction motors based on quaternion analysis. *Measurement* 222, 113680. doi:10.1016/j.measurement.2023.113680

Chen, L., Shen, J., Xu, G., Chi, C., Feng, Q., Zhou, Y., et al. (2023). Induction motor stator winding inter-tern short circuit fault detection based on start-up current envelope energy. *Sensors* 23, 8581. doi:10.3390/s23208581

Chen, R., Shen, C., Sheng, T., and Zhao, Y. (2024). Inter-turn short-circuit diagnosis of wound-field doubly salient machine using multi-signal fusion and ga-xgboost. *Front. Signal Process.* 4, 4–2024. doi:10.3389/frsip.2024.1433831

de Souza, D. F., Salotti, F. A. M., Sauer, I. L., Tatizawa, H., de Almeida, A. T., and Kanashiro, A. G. (2022). A performance evaluation of three-phase induction electric motors between 1945 and 2020. *Energies* 15, 2002. doi:10.3390/en15062002

Dias, C. G., da Silva, L. C., and Luz Alves, W. A. (2020). A histogram of oriented gradients approach for detecting broken bars in squirrel-cage induction motors. *IEEE Trans. Instrum. Meas.* 69, 6968–6981. doi:10.1109/TIM.2020.2975388

Dias, C. G., Rodrigues, K. L., Menegasse, N. C., Alves, W. A. L., and Silva, L. C. d. (2023). Histogram of oriented gradients for rotor speed estimation in three-phase induction motors. *IEEE Trans. Instrum. Meas.* 72, 1–11. doi:10.1109/TIM.2023.3276530

Faraj, H. Z., Al-Dujaili, A. Q., and Humaidi, A. J. (2023). "The classification method of electrical faults in permanent magnet synchronous motor based on deep learning," in 2023 IEEE 11th Conference on Systems, Process and Control (ICSPC), 326–331. doi:10.1109/ICSPC59664.2023.10420154

Gangeh, M. J., Farahat, A. K., Ghodsi, A., and Kamel, M. S. (2015). Supervised dictionary learning and sparse representation-a review. *arXiv Preprint arXiv:1502.05928*. doi:10.48550/arXiv.1502.05928

Gangsar, P., and Tiwari, R. (2020). Signal based condition monitoring techniques for fault detection and diagnosis of induction motors: a state-of-the-art review. *Mech. Syst. Signal Process.* 144, 106908. doi:10.1016/j.ymssp.2020.106908

Garcia-Calva, T., Morinigo-Sotelo, D., Fernandez-Cavero, V., and Romero-Troncoso, R. (2022). Early detection of faults in induction motors–a review. *Energies* 15, 7855. doi:10.3390/en15217855

Ge, X., Yang, F., Zhu, H., Zeng, X., and Zhou, D. (2019). An efficient fpga implementation of orthogonal matching pursuit with square-root-free qr decomposition. *IEEE Trans. Very Large Scale Integration (VLSI) Syst.* 27, 611–623. doi:10.1109/TVLSI.2018.2879884

Ghanbari, T., Mehraban, A., and Farjah, E. (2022). Inter-turn fault detection of induction motors using a method based on spectrogram of motor currents. *Measurement* 205, 112180. doi:10.1016/j.measurement.2022.112180

Ghosh, P. K., Sadhu, P. K., Basak, R., and Sanyal, A. (2020). Energy efficient design of three phase induction motor by water cycle algorithm. *Ain Shams Eng. J.* 11, 1139–1147. doi:10.1016/j.asej.2020.01.017

Glucina, M., Andelic, N., Lorencin, I., and Car, Z. (2023). Estimation of excitation current of a synchronous machine using machine learning methods. *Computers* 12. doi:10.3390/computers12010001

Gonzalez-Abreu, A.-D., Osornio-Rios, R.-A., Jaen-Cuellar, A.-Y., Delgado-Prieto, M., Antonino-Daviu, J.-A., and Karlis, A. (2022). Advances in power quality analysis techniques for electrical machines and drives: a review. *Energies* 15, 1909. doi:10.3390/en15051909

Gyftakis, K. N. (2022). A comparative investigation of interturn faults in induction motors suggesting a novel transient diagnostic method based on the goerges phenomenon. *IEEE Trans. Industry Appl.* 58, 304–313. doi:10.1109/TIA.2021.3131296

Gyftakis, K. N., and Cardoso, A. J. M. (2021). Reliable detection of stator interturn faults of very low severity level in induction motors. *IEEE Trans. Industrial Electron.* 68, 3475–3484. doi:10.1109/TIE.2020.2978710

He, Y., Li, G., Liao, Y., Sun, Y., Kong, J., Jiang, G., et al. (2019). Gesture recognition based on an improved local sparse representation classification algorithm. *Clust. Comput.* 22, 10935–10946. doi:10.1007/s10586-017-1237-1

Hussain, M., Kumar, D., Kalwar, I. H., Memon, T. D., Memon, Z. A., Nisar, K., et al. (2021). Stator winding fault detection and classification in three-phase induction motor. *Intell. Autom. Soft Comput.* 29, 869–883. doi:10.32604/iasc.2021.017790

Jiménez-Guarneros, M., Morales-Perez, C., and Rangel-Magdaleno, J. d. J. (2022). Diagnostic of combined mechanical and electrical faults in asd-powered induction motor using modwt and a lightweight 1-d cnn. *IEEE Trans. Industrial Inf.* 18, 4688–4697. doi:10.1109/TII.2021.3120975

Leon-Garcia, A. (2017). *Probability, statistics, and random processes for electrical engineering*. Upper Saddle River, NJ: Pearson Prentice Hall.

Li, J., Chow, P., Peng, Y., and Jiang, T. (2021). Fpga implementation of an improved omp for compressive sensing reconstruction. *IEEE Trans. Very Large Scale Integration (VLSI) Syst.* 29, 259–272. doi:10.1109/TVLSI.2020.3030906

Marcot, B. G., and Hanea, A. M. (2021). What is an optimal value of k in k-fold cross-validation in discrete bayesian network analysis? *Comput. Stat.* 36, 2009–2031. doi:10.1007/s00180-020-00999-9

Mejia-Barron, A., de Santiago-Perez, J. J., Granados-Lieberman, D., Amezquita-Sanchez, J. P., and Valtierra-Rodriguez, M. (2019). Shannon entropy index and a fuzzy logic system for the assessment of stator winding short-circuit faults in induction motors. *Electronics* 8. doi:10.3390/electronics8010090

Morales-Perez, C., Rangel-Magdaleno, J., Peregrina-Barreto, H., Amezquita-Sanchez, J. P., and Valtierra-Rodriguez, M. (2018). Incipient broken rotor bar detection in induction motors using vibration signals and the orthogonal matching pursuit algorithm. *IEEE Trans. Instrum. Meas.* 67, 2058–2068. doi:10.1109/TIM.2018.2813820

Morales-Perez, C. J., de Jesus Rangel-Magdaleno, J., Peregrina-Barreto, H., Garcia-Perez, A., and Ramirez-Cortes, J. M. (2022). Noise reduction in electrical signal using omp algorithm based on dct and dsc dictionaries. *IEEE Trans. Instrum. Meas.* 71, 1–11. doi:10.1109/TIM.2021.3135319

Niu, G., Dong, X., and Chen, Y. (2023). Motor fault diagnostics based on current signatures: a review. *IEEE Trans. Instrum. Meas.* 72, 1–19. doi:10.1109/TIM.2023.3285999

Prakash, R. B. R., rao Ranga, M., Pandian, A., and Varma, P. S. (2020). Induction machine stator winding failure detection using motor current signature analysis. *IOP Conf. Ser. Mater. Sci. Eng.* 993, 012084. doi:10.1088/1757-899X/993/1/012084

Qu, N., Wang, J., and Liu, J. (2019). An arc fault detection method based on current amplitude spectrum and sparse representation. *IEEE Trans. Instrum. Meas.* 68, 3785–3792. doi:10.1109/TIM.2018.2880939

Rajamany, G., Srinivasan, S., Rajamany, K., and Natarajan, R. K. (2019). Induction motor stator interturn short circuit fault detection in accordance with line current sequence components using artificial neural network. *J. Electr. Comput. Eng.* 2019, 1–11. doi:10.1155/2019/4825787

Rani, M., Dhok, S. B., and Deshmukh, R. B. (2018). A systematic review of compressive sensing: concepts, implementations and applications. *IEEE Access* 6, 4875–4894. doi:10.1109/ACCESS.2018.2793851

Roy, S., Acharya, D. P., and Sahoo, A. K. (2019). Low-complexity architecture of orthogonal matching pursuit based on qr decomposition. *IEEE Trans. Very Large Scale Integration (VLSI) Syst.* 27, 1623–1632. doi:10.1109/TVLSI.2019.2909754

Roy, S., Acharya, D. P., and Sahoo, A. K. (2021). Fast omp algorithm and its fpga implementation for compressed sensing-based sparse signal acquisition systems. *IET Circuits, Devices and Syst.* 15, 511–521. doi:10.1049/cds2.12047

Sadeghi, M., Babaie-Zadeh, M., and Jutten, C. (2013). Dictionary learning for sparse representation: a novel approach. *IEEE Signal Process. Lett.* 20, 1195–1198. doi:10.1109/LSP.2013.2285218

Sakhara, S., Saad, S., and Nacib, L. (2017). Diagnosis and detection of short circuit in asynchronous motor using three-phase model. *Int. Journal System Assurance Engineering Management* 8, 308–317. doi:10.1007/s13198-016-0435-1

Sarkar, S., Purkait, P., and Das, S. (2021). Ni compactrio-based methodology for online detection of stator winding inter-turn insulation faults in 3-phase induction motors. *Measurement* 182, 109682. doi:10.1016/j.measurement.2021.109682

Sheikh, M. A., Bakhsh, S. T., Irfan, M., Nor, N. b. M., and Nowakowski, G. (2022). A review to diagnose faults related to three-phase industrial induction motors. *J. Fail. Analysis Prev.* 22, 1546–1557. doi:10.1007/s11668-022-01445-2

Shih, K.-J., Hsieh, M.-F., Chen, B.-J., and Huang, S.-F. (2022). Machine learning for inter-turn short-circuit fault diagnosis in permanent magnet synchronous motors. *IEEE Trans. Magnetics* 58, 1–7. doi:10.1109/TMAG.2022.3169173

Susanta Ray, B. G., and Dey, D. (2020). Identification and classification of stator inter-turn faults in induction motor using wavelet kernel based convolutional neural network. *Electr. Power Components Syst.* 48, 1421–1432. doi:10.1080/15325008.2020.1854384

Tang, H., Dai, H.-L., and Du, Y. (2022). Bearing fault detection for doubly fed induction generator based on stator current. *IEEE Trans. Industrial Electron.* 69, 5267–5276. doi:10.1109/TIE.2021.3080216

Terron-Santiago, C., Martinez-Roman, J., Puche-Panadero, R., and Sapena-Bano, A. (2021). A review of techniques used for induction machine fault modelling. *Sensors* 21, 4855. doi:10.3390/s21144855

Villalobos-Pina, F. J., Reyes-Malanche, J. A., Cabal-Yepez, E., and Ramirez-Velasco, E. (2024). "Electric fault diagnosis in induction machines using motor current signature analysis (MCSA)," in *Time series analysis - recent advances, new perspectives and applications*. Editors P. J. Rocha, S. Oliveira, and D. C. M. Viana (London, United Kingdom: IntechOpen). doi:10.5772/intechopen.1004002

Wang, J. (2015). Support recovery with orthogonal matching pursuit in the presence of noise. *IEEE Trans. Signal Process.* 63, 5868–5877. doi:10.1109/TSP.2015.2468676

Wang, L., Liu, H., Liang, J., Zhang, L., Ji, Q., and Wang, J. (2022). Research on the rotor fault diagnosis method based on qpso-vmd-pca-svm. *Front. Energy Res.* 10, 10–2022. doi:10.3389/fenrg.2022.944961

Wu, R., Huang, W., and Chen, D.-R. (2013). The exact support recovery of sparse signals with noise *via* orthogonal matching pursuit. *IEEE Signal Process. Lett.* 20, 403–406. doi:10.1109/LSP.2012.2233734

Zhang, Z., Xu, Y., Yang, J., Li, X., and Zhang, D. (2015). A survey of sparse representation: algorithms and applications. *IEEE Access* 3, 490–530. doi:10.1109/ACCESS.2015.2430359

Zhao, C., Feng, Z., Wei, X., and Qin, Y. (2018). Sparse classification based on dictionary learning for planet bearing fault identification. *Expert Syst. Appl.* 108, 233–245. doi:10.1016/j.eswa.2018.05.012

Ziad, H., Al-Dujaili, A., and Humaidi, A. (2024). Techniques used in faults detection of permanent magnet synchronous motor: a review. *AIP Conf. Proc.* 3232, 030004. doi:10.1063/5.0236292

Ziad, H., Al-Dujaili, A. Q., and Humaidi, A. J. (2025). A comparative study of deep learning efficiency in the classification of electrical faults of permanent magnet synchronous motor. *Int. Rev. Appl. Sci. Eng.* 16, 292–302. doi:10.1556/1848.2024.00885